Structural Safety 76 (2019) 81–94

Contents lists available at ScienceDirect

Structural Safety

journal homepage: www.elsevier.com/locate/strusafe

System-reliability-based design and topology optimization of structures under constraints on first-passage probability

Junho Chun[a], Junho Song[b,*], Glaucio H. Paulino[c]

[a] School of Architecture, Syracuse University, Syracuse, NY, United States
[b] Department of Civil and Environmental Engineering, Seoul National University, Seoul, Republic of Korea
[c] School of Civil and Environmental Engineering, Georgia Institute of Technology, Atlanta, GA, United States

ARTICLE INFO

Keywords:
Reliability-based design optimization
Reliability-based topology optimization
Stochastic excitation
Sequential compounding method
Parameter sensitivity
System reliability
First-passage probability

ABSTRACT

For the purpose of reliability assessment of a structure subject to stochastic excitations, the probability of the occurrence of at least one failure event over a time interval, i.e. the first-passage probability, often needs to be evaluated. In this paper, a new method is proposed to incorporate constraints on the first-passage probability into reliability-based optimization of structural design or topology. For efficient evaluations of first-passage probability during the optimization, the failure event is described as a series system event consisting of instantaneous failure events defined at discrete time points. The probability of the series system event is then computed by use of a system reliability analysis method termed as the sequential compounding method. The adjoint sensitivity formulation is derived for calculating the parameter sensitivity of the first-passage probability to facilitate the use of efficient gradient-based optimization algorithms. The proposed method is successfully demonstrated by numerical examples of a space truss and building structures subjected to stochastic earthquake ground motions.

1. Introduction

Finding the optimal design of a structural system with regard to safety, cost or performance is one of the most essential tasks in structural engineering practice. The optimal design should achieve major design objectives representing reliable operation and safety even under stochastic excitations caused by natural hazards such as earthquakes and wind loads. Due to inherent randomness in natural disasters, however, significant uncertainties may exist in the intensity and characteristics of the excitations. Therefore, the performance of such structural systems needs to be assessed probabilistically during the optimization process.

To deal with uncertainties effectively in structural design/topology optimization, various optimization algorithms and frameworks were developed recently. For instance, the so-called *robust* design/topology optimization algorithms [1–3] aim to reduce the sensitivity of the optimal performance of a structure with respect to the randomness of interest. By contrast, *Reliability-based* design/topology optimization [4–10] aims to find optimal solutions satisfying the probabilistic constraints on the structural performance indicators. So far, these studies have been mainly focusing on accounting for uncertainties in *static* loads representing typical load patterns of the structure. Recent studies on structural optimization considering dynamic excitations employed a small number of deterministic time histories representing possible future realizations [11,12], or focused on partial descriptors of the dynamic responses such as mode frequencies [13]. These approaches have intrinsic limitations because (1) a single or small number of sample time histories may not represent all possible realizations of stochastic excitations, and (2) it is practically impossible to assess the probabilities that the structural design does not satisfy the constraints on performances, i.e. failure probabilities using this approach. Therefore, the probabilistic prediction of structural responses based on random vibration analysis is needed in the process for optimal design.

To overcome this technical challenge, the authors recently proposed a new method for topology optimization of structures under stochastic excitations [14]. In the proposed method, an efficient random vibration analysis method based on the use of the discrete representation method [15] and structural reliability theories (see [16] for a review) were integrated within a state-of-the-art topology optimization framework. The authors also developed a system reliability-based topology optimization framework under stochastic excitations [17] to cope with *system* failure events consisting of statistical dependent component events using the matrix-based system reliability method [18]. The developed method helps satisfy probabilistic constraints on a system

* Corresponding author.
E-mail address: junhosong@snu.ac.kr (J. Song).

https://doi.org/10.1016/j.strusafe.2018.06.006
Received 5 September 2017; Accepted 17 June 2018

failure event, which consists of multiple limit-states defined in terms of different locations, failure modes or time points as it optimizes a structural system.

In these studies by the authors, the *instantaneous* failure probabilities of the structure were evaluated at discrete time points. However, to promote applications of design/topology optimization to engineering design practice, the first-passage probability, i.e. the probability of at least one occurrence of the failure over a time interval, needs to be estimated during the optimization process. Spence et al. [19] proposed a framework for RBDO of linear systems constrained on the first-passage probability. This approach decouples the nested reliability analysis loop from the optimization loop by solving sub-optimization problem formulated from simulation results. Bobby et al. [20] presented a simulation-based framework for topology optimization of wind-excited building structures with the consideration of the first-passage probability.

The first-passage probability helps promote the use of the proposed stochastic optimization framework for the design of the lateral load-resisting system or sizing structural elements under stochastic excitations with a finite duration such as earthquake excitations. To this end, this paper introduces a stochastic design and topology optimization method that can handle probabilistic constraints on the first-passage probability, and demonstrates the method using numerical examples.

2. Random vibration analysis using discrete representation method

In the aforementioned reliability-based design optimization framework under stochastic excitations [14,17], the authors proposed to perform random vibration analysis by use of the discrete representation method [15] in order to compute the instantaneous failure probability of the stochastic response at discrete time points. In the proposed approach, for example, a zero-mean stationary Gaussian input excitation process $f(t)$ is discretized as

$$f(t) = \sum_{i=1}^{n} v_i s_i(t) = \mathbf{s}(t)^{\mathrm{T}}\mathbf{v} \tag{1}$$

where $\mathbf{s}(t)$ $(= [s_1(t),\ldots, s_n(t)]^{\mathrm{T}})$ is a vector of deterministic functions that describe the spectral characteristics of the process, and $\mathbf{v} = [v_1, v_2,\ldots, v_n]^{\mathrm{T}}$ is a vector of uncorrelated standard normal random variables. Among existing methods available to develop a discrete representation model in Eq. (1), a popular one for ground excitation modeling is using a filter representing the characteristic of the soil medium and a random pulse train. For example, if a filtered white noise is used, the model in Eq. (1) is constructed as

$$f(t) = \int_0^t h_f(t-\tau)W(\tau)d\tau = \mathbf{s}(t)^{\mathrm{T}}\mathbf{v}$$
$$s_i(t) = \begin{cases} \sqrt{2\pi\Phi_0/\Delta t}\cdot\int_{t_{i-1}}^{t_i} h_f(t-\tau)d\tau & t_{i-1} < t < t_i,\ i = 1,\ldots,n \\ 0 & t \leqslant t_{i-1} \end{cases} \tag{2}$$

in which $W(\tau)$ denotes the white noise process whose power spectral density function is $\Phi_{WW}(\omega) = \Phi_0$, $h_f(\cdot)$ is the impulse response function of the filter, $\Delta t = t_i - t_{i-1}$, and n denotes the number of the time intervals introduced for the given time period $(0, t)$. The details of the derivation of Eq. (2) are available in Chun et al. [14].

2.1. Response of linear system under stochastic excitations

The responses of linear systems to stochastic excitation can be determined by the convolution integral consisting of their impulse response function and the discretized input process in Eq. (1). That is, a response time history $u(t)$ of the linear system subjected to the stochastic excitation $f(t)$ is derived as

$$u(t) = \int_0^t f(\tau)h_s(t-\tau)d\tau = \int_0^t \sum_{i=1}^{n} v_i s_i(\tau)h_s(t-\tau)d\tau = \sum_{i=1}^{n} v_i a_i(t)$$
$$= \mathbf{a}(t)^{\mathrm{T}}\mathbf{v} \tag{3}$$

where $h_s(\cdot)$ is the impulse response function of the linear structural system, and $\mathbf{a}(t)$ denotes a vector of deterministic basis functions

$$a_i(t) = \int_0^t s_i(\tau)h_s(t-\tau)d\tau, \quad i = 1,\ \ldots, n \tag{4}$$

Deriving the impulse response function in a finite element setting can be computationally challenging or cumbersome. To facilitate the process, the authors proposed novel numerical procedures in Chun et al. [14].

2.2. Instantaneous failure probability of linear system under stochastic excitations

In structural reliability analysis, the probability that the outcome of a random vector $\mathbf{X}$ is located inside the failure domain Ω_f, i.e. the failure probability, is computed by an integral

$$P_f = \int_{\Omega_f} f_{\mathbf{X}}(\mathbf{x})d\mathbf{x} \tag{5}$$

where $f_{\mathbf{X}}(\mathbf{x})$ is the joint probability density function (PDF) of the random vector $\mathbf{X}$. The failure domain is defined by the area where the limit-state function $g(\mathbf{x})$, e.g. capacity minus demand, takes the negative sign. In general, computing the multi-fold integral in Eq. (5) is non-trivial or computationally challenging. Structural reliability methods such as FORM and SORM (see [16] for a review) transform the space of the random variable $\mathbf{x}$ into the uncorrelated standard normal space $\mathbf{v}$. Then, the limit-state function is approximated by a linear (FORM) or quadratic function (SORM) at the design point, often alternatively termed as the most probable failure point (MPP). For example, in FORM, the failure probability is approximated as

$$P_f = \Phi[-\beta] \tag{6}$$

where β is the reliability index, i.e. the shortest distance from the origin of the standard normal space to the linearized failure surface, and $\Phi[\cdot]$ denotes the cumulative distribution function (CDF) of the standard normal distribution. Using the discrete representation method described above, limit-state functions defined for displacement or other structural responses can be described in the space of standard normal random variable $\mathbf{v}$. For example, the instantaneous failure event E_f defined for a linear structure subjected to the Gaussian input process in Eq. (1) is given by

$$E_f(t_k, u_0, \mathbf{v}) = \{g(t_k, u_0, \mathbf{v}) \leqslant 0\}, \quad \text{where } g(t_k, u_0, \mathbf{v}) = u_0 - u(t_k)$$
$$= u_0 - \mathbf{a}(t_k)^{\mathrm{T}}\mathbf{v} \tag{7}$$

where u_0 is the prescribed threshold on the displacement response. In this case, the reliability index β is computed from the geometric interpretation of the limit-state surface as a closed form expression [15]

$$\beta(t_k, u_0) = \frac{u_0}{\|\mathbf{a}(t_k)\|} \tag{8}$$

It is noted that the limit-state function in Eq. (7) is linear in this case, and thus the failure probability by Eq. (6), i.e. $P_f = \Phi[-\beta(t_k,u_0)]$ does not introduce errors caused by function approximation or require nonlinear optimization to find the design point. If the structure behaves nonlinearly or the input process is non-Gaussian, one needs to use reliability methods such as FORM or SORM to compute the failure probability approximately. Using this discrete representation method, one can reduce the computational cost of the random vibration analysis, which should be repetitively performed during the optimization processes to compute the instantaneous failure probability at each updated set of design variables.

2.3. First-passage probability of linear system under stochastic excitations

The first-passage probability is commonly utilized to find the probability of the failure event described within a time interval [21–23]. One of the available approaches for formulating the first-passage probability P_{fp} defines the problem as a series system problem, i.e.

$$P_{fp} = P(u_0 < \max_{0<t<t_n} u(t)) = P\left(\bigcup_{k=1}^{n} \{u(t_k) > u_0\}\right) \tag{9}$$

Using the discrete representation, the first-passage probability of a system with n_c limit-state functions (defined for different failure modes or locations) is described as

$$P_{fp} = P\left(\bigcup_{i=1}^{n_c} E_{sys}^{i}\right) = P\left(\bigcup_{i=1}^{n_c}\bigcup_{k=1}^{n} E_{f_i}(t_k, u_0, \mathbf{v})\right) \tag{10}$$

where E_{sys}^{i} denotes the first-passage failure event regarding the i-th constraint, $E(\cdot)$ denotes the instantaneous failure event of the i-th limit-state function at time t_k, and n is the total number of discretized time points. To compute the first-passage probability in Eq. (10), it is required to evaluate the failure probabilities of the component events at each time point within an interval. Moreover, an efficient, reliable and robust algorithm is required to evaluate the system failure probability with a proper consideration of statistical dependency between the component events. It is also desirable to compute the parameter sensitivity of the series system failure probabilities in Eqs. (9) and (10) to enable the use of efficient gradient-based optimizers. To address these requirements, the sequential compounding method (SCM; [24]) and the Chun-Song-Paulino (CSP; [25]) method are adopted in this study.

3. Optimization of structures subjected to stochastic excitation under first-passage probability constraints

3.1. Structural design optimization

Reliability Based Design Optimization (RBDO) of a structure aims to achieve the optimal design under probabilistic constraints on uncertain performance, arising from uncertainties in material properties or loads. The RBDO problem of a structure under first-passage probability constraints can be formulated as a System Reliability Based Design Optimization (SRBDO) problem [9], i.e.

$$\begin{aligned}
&\min_{\mathbf{d}} f_{obj}(\mathbf{d})\\
&s.t \quad P(E_{sys}^{i}) = P\left(\bigcup_{k=1}^{n} E_{f_i}(t_k, \mathbf{d})\right)\\
&\qquad = P\left(\bigcup_{k=1}^{n} \{g_i(t_k, \mathbf{d}) \leqslant 0\}\right) \leqslant P_{f_i}^{\text{target}}, \quad i = 1,\ldots,n_c\\
&\qquad \mathbf{d}^{\text{lower}} \leqslant \mathbf{d} \leqslant \mathbf{d}^{\text{upper}}\\
&\text{with } \mathbf{M}(\mathbf{d})\ddot{\mathbf{u}}(t, \mathbf{d}) + \mathbf{C}(\mathbf{d})\dot{\mathbf{u}}(t, \mathbf{d}) + \mathbf{K}(\mathbf{d})\mathbf{u}(t, \mathbf{d}) = \mathbf{f}(t, \mathbf{d})
\end{aligned} \tag{11}$$

where $f_{obj}(\mathbf{d})$ denotes the objective function of the design, $\mathbf{d}^{\text{lower}}$ and $\mathbf{d}^{\text{upper}}$ are the lower and upper bounds of the vector of design variables $\mathbf{d}$, respectively. $g_i(\,)$ represents the limit-state function whose negative sign indicates the violation of a given constraint, n_c is the number of the constraints, $P(g_i(\cdot) \leq 0)$ is the probability of the failure event, and P_f^{target} is the target failure probability.

$\mathbf{M}$, $\mathbf{C}$, and $\mathbf{K}$ represent the global mass, damping and stiffness matrices of the structure, respectively, and $\ddot{\mathbf{u}}$, $\dot{\mathbf{u}}$, $\mathbf{u}$, and $\mathbf{f}$ are the acceleration, velocity, displacement and force vectors at time t, respectively. A proportional damping model known as 'Rayleigh damping' [26] is used throughout this paper. In this approach, the damping matrix is determined as a linear combination of the stiffness and mass matrix, that is $\mathbf{C} = \kappa_0\mathbf{M} + \kappa_1\mathbf{K}$. The coefficients κ_0 and κ_1 in the Rayleigh damping model are determined so as to have certain modal damping factors. For earthquake ground excitations, the force vector in Eq. (11) is determined by a vector of effective earthquake forces, i.e.

$$\mathbf{f}(t, \mathbf{d}) = -\mathbf{M}(\mathbf{d})\mathbf{l}\ddot{u}_g(t) = -\mathbf{M}(\mathbf{d})\mathbf{l}f(t) \tag{12}$$

where $\mathbf{l}$ represents the directional distribution of mass with unity resulting from a unit ground displacement and $\ddot{u}_g$ is the ground acceleration time history.

3.2. Structural topology optimization

Topology optimization (see [27] for a review) aims to find the optimal material distributions in a design domain subjected to tractions and displacement boundary conditions while satisfying given design constraints. Thus, every point of a design domain is expected to represent either an existence of material or a void region. The Solid Isotropic Material with Penalization (SIMP; [28]) model, which is adopted in this study, considers a continuous material density in a design variable using the power function representation, i.e.

$$\psi(x) = x^p \tag{13}$$

where p is the penalization factor and x is a density associated with element e in the finite element method setting. The topology optimization solutions using the SIMP, or related models, may suffer from "checkerboard" patterns and mesh-dependency [29]. To overcome these problems, various methods have been proposed (e.g. [30–33]). In this study, a projection method [30] is implemented to obtain a filtered density based on element design variables within the neighborhood such as:

$$\widetilde{\rho}_e = \frac{\sum_{j\in\mathbb{N}_e} w(r_j)d_j}{\sum_{j\in\mathbb{N}_e} w(r_j)}, \quad w(r_j) = \begin{cases} \frac{r_{\min} - r_j}{r_{\min}} & \text{if } r_{\min} \geqslant r_j \\ 0 & \text{otherwise} \end{cases} \tag{14}$$

where d_j denotes design variable of element j, $\mathbb{N}_e$ represents the set of elements within the radius $r_{\min}$ of element e, $w(r_j)$ is the weighting function, and r_j is the distance between the centroids of element j and e.

Using the SIMP model, the stiffness and mass matrix of element e and their derivatives with respect to an element density are obtained as follows in the element-based computational framework [27]:

$$\begin{aligned}
&\mathbf{K}_e(\widetilde{\rho}_e) = \widetilde{\rho}_e^{\,p}\mathbf{K}_e^0, \quad \mathbf{M}_e(\widetilde{\rho}_e) = \widetilde{\rho}_e^{\,q}\mathbf{M}_e^0\\
&\frac{\partial \mathbf{K}_e(\widetilde{\rho}_e)}{\partial \widetilde{\rho}_e} = p\widetilde{\rho}_e^{\,p-1}\mathbf{K}_e^0, \quad \frac{\partial \mathbf{M}_e(\widetilde{\rho}_e)}{\partial \widetilde{\rho}_e} = q\widetilde{\rho}_e^{\,q-1}\mathbf{M}_e^0
\end{aligned} \tag{15}$$

where q is the penalization parameter, and $\mathbf{K}_e^0$ and $\mathbf{M}_e^0$ are computed by

$$\mathbf{K}_e^0 = \int_{\Omega_e} \mathbf{B}^{\mathrm{T}}\mathbf{D}_0\mathbf{B}\Omega_e, \quad \mathbf{M}_e^0 = \int_{\Omega_e} \mathbf{N}^{\mathrm{T}}\rho_m\mathbf{N}d\Omega_e \tag{16}$$

where $\mathbf{B}$ denotes the strain–displacement matrix of the shape function derivatives in the domain Ω_e of element e, ρ_m represents the mass density of the material and $\mathbf{N}$ is the shape function of element e. $\mathbf{D}_0$ is the elasticity tensor of the solid material, where the density is 1.

Topology optimization of a structure under stochastic excitation with constraints on the first-passage probability can be formulated as

$$\begin{aligned}
&\min_{\mathbf{d}} \; f_{obj}(\widetilde{\boldsymbol{\rho}})\\
&s.\,t \quad P(E_{sys}^{i}) = P\left(\bigcup_{k=1}^{n} E_{f_i}(t_k, \widetilde{\boldsymbol{\rho}})\right)\\
&\qquad = P\left(\bigcup_{k=1}^{n} \{g_i(t_k, \widetilde{\boldsymbol{\rho}}) \leqslant 0\}\right) \leqslant P_{f_i}^{\text{target}}, \; i = 1,\ldots,n_c\\
&\qquad 0 < \varepsilon \leqslant \widetilde{\rho}_i \leqslant 1 \;\; \forall\, i \in \Omega\\
&\text{with } \mathbf{M}(\widetilde{\boldsymbol{\rho}})\ddot{\mathbf{u}}(t, \widetilde{\boldsymbol{\rho}}) + \mathbf{C}(\widetilde{\boldsymbol{\rho}})\dot{\mathbf{u}}(t, \widetilde{\boldsymbol{\rho}}) + \mathbf{K}(\widetilde{\boldsymbol{\rho}})\mathbf{u}(t, \widetilde{\boldsymbol{\rho}}) = \mathbf{f}(t, \widetilde{\boldsymbol{\rho}})
\end{aligned} \tag{17}$$

where $\mathbf{d}$ denotes the vector of design variables, Ω is a set of finite element indices and $\widetilde{\boldsymbol{\rho}}$ is the vector of filtered densities defined as:

$$\widetilde{\boldsymbol{\rho}} = \mathbf{P}\mathbf{d} \tag{18}$$

where $\mathbf{P}$ represents the filtering matrix whose element is determined by

$$(\mathbf{P})_{lk} = \frac{w_{lk}}{\sum_{j\in\bar{\mathbb{N}}_l} w(r_j)}, \quad w_{lk} = \begin{cases} w(r_k) & \text{if } k \in \bar{\mathbb{N}}_l \\ 0 & \text{otherwise} \end{cases} \tag{19}$$

A flowchart for topology optimization of a structure constrained by first-passage probability is provided in Appendix A.

Various engineering constraints can be incorporated into the above formulations of reliability-based design optimization and topology optimization under first-passage probability. To promote applications of the proposed method to truss and building structures, engineering constraints on stress in the bar and inter-story drift ratio are derived below.

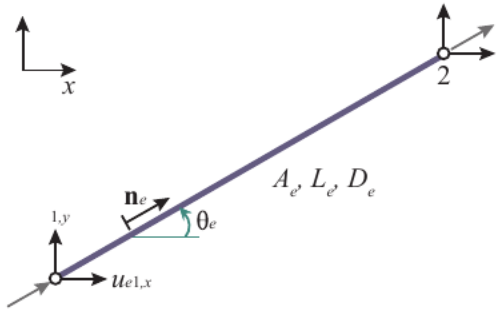

Fig. 1. Bar geometry.

3.3. First-passage probability constraints on stress in bar elements

Consider a bar e in a truss structure with the local node numbers 1 and 2 denoting the end points of the bar as shown in Fig. 1. A unit vector $\mathbf{n}_e$ pointing from node 1 to node 2 is defined as

$$\mathbf{n}_e = \begin{pmatrix} \cos\theta_e \\ \sin\theta_e \end{pmatrix} \tag{20}$$

The global displacement vectors of the end nodes of bar e are written as

$$\mathbf{u}_e = \begin{pmatrix} \mathbf{u}^g_{e1} \\ \mathbf{u}^g_{e2} \end{pmatrix}, \text{ where } \mathbf{u}^g_{e1} = \begin{pmatrix} u_{e1,x} \\ u_{e1,y} \end{pmatrix}, \quad \mathbf{u}^g_{e2} = \begin{pmatrix} u_{e2,x} \\ u_{e2,y} \end{pmatrix} \tag{21}$$

The stress (t) in a truss element e under stochastic excitations can be computed from the stress–strain relationship based on Hooke's law as follows:

$$\sigma_e(t, \mathbf{d}) = \frac{D_e}{L_e}\mathbf{n}_e\cdot(\mathbf{u}^g_{e2}(t, \mathbf{d}) - \mathbf{u}^g_{e1}(t, \mathbf{d})) = \frac{D_e}{L_e}\mathbf{B}_e\mathbf{u}_e = \frac{D_e}{L_e}(u^l_{e2}(t, \mathbf{d}) - u^l_{e1}(t, \mathbf{d})) \tag{22}$$

where D_e denotes Young's modulus, L_e is the length of the element e, $u^l_{e1}(t)$ and $u^l_{e2}(t)$ are end displacements along the truss axis, and

$$\mathbf{B}_e = [-\mathbf{n}_e^{\mathrm{T}}\ \mathbf{n}_e^{\mathrm{T}}] \tag{23}$$

The elongation in Eq. (22) can be described by using the discrete representation form in Eq. (3), i.e.

$$\sigma_e(t, \mathbf{d}) = \frac{D_e}{L_e}(\mathbf{a}(t, \mathbf{d})^{\mathrm{T}}_{e2}\mathbf{v} - \mathbf{a}(t, \mathbf{d})^{\mathrm{T}}_{e1}\mathbf{v}) \tag{24}$$

The instantaneous failure probability at time t_k is expressed in terms of stress in the truss element e as

$$P(E_{fe}(t_k, \mathbf{d})) = P(g_e(t_k, \mathbf{d}) \leqslant 0) = P(\sigma_{0e} - \sigma_e(t_k, \mathbf{d}) \leqslant 0) = \Phi[-\beta_{\sigma e}(t_k, \mathbf{d})] \tag{25}$$

where $_{0e}$ denotes the threshold value of stress. From the geometric representation associated with the failure event of element e, the reliability index at time t_k is computed as

$$\beta_{\sigma e}(t_k, \mathbf{d}) = \frac{L_e\cdot\sigma_{0e}}{D_e\|\mathbf{a}(t_k, \mathbf{d})^{\mathrm{T}}_{e1} - \mathbf{a}(t_k, \mathbf{d})^{\mathrm{T}}_{e2}\|} = \frac{L_e\cdot\sigma_{0e}}{D_e\|\mathbf{b}_e(t_k, \mathbf{d})\|} \tag{26}$$

The first-passage probability of the stress limit state function is then computed as

$$\begin{aligned} P_{fp\_\sigma}(E_{sys}) &= P\left(\bigcup_{k=1}^{n} E_{f\sigma}(t_k, \mathbf{d})\right) = P\left(\bigcup_{k=1}^{n}\{\sigma_{0e} - \sigma_e(t_k, \mathbf{d}) \leqslant 0\}\right) \\ &= 1 - \Phi_n[\beta_{\sigma e}(t_1, \mathbf{d}), \beta_{\sigma e}(t_2, \mathbf{d}), \ldots, \beta_{\sigma e}(t_n, \mathbf{d}); \rho_{1,2}, \rho_{1,3}, \ldots, \rho_{n-1,n}] \\ &= 1 - \Phi_n[\boldsymbol{\beta}_{\sigma e}, \mathbf{R}] \end{aligned} \tag{27}$$

where Φ_n denotes the multivariate normal CDF, $_{i,j}$ represents the correlation coefficient between the normal random variables representing failure event i and j, and and $\mathbf{R}$ are the vectors of the reliability indices and the correlation coefficient matrix, respectively. The correlation coefficient matrix $\mathbf{R}$ is constructed as

$$\mathbf{R} = \begin{bmatrix} \rho_{1,1} & \cdots & \rho_{1,n} \\ \vdots & \ddots & \vdots \\ \rho_{n,1} & \cdots & \rho_{n\,n} \end{bmatrix}, \quad \rho_{k,l} = \boldsymbol{\alpha}(t_k)^{\mathrm{T}}\cdot\boldsymbol{\alpha}(t_l) \tag{28}$$

where $(t_i) = \mathbf{a}(t_i)/||\mathbf{a}(t_i)||$ denotes the negative normalized gradient vector of the limit-state function evaluated at the design point which is obtained by $u_0\cdot\mathbf{a}(t_i)/||\mathbf{a}(t_i)||^2$. The multivariate CDF in Eq. (27) and those in the following Sections 3.4 and 3.5 are computed by SCM [24]. The CSP method [25] whose details are presented in Section 5 is used to compute the sensitivity of the multivariate CDF.

3.4. First-passage probability constraint on inter-story drift ratio

The first-passage probability can be computed in terms of the inter-story drift ratio, which is one of the significant design criteria in structural engineering, defined as

$$\frac{\Delta_i(t, \mathbf{d})}{H_i} = \begin{cases} \dfrac{\mathbf{a}(t, \mathbf{d})_i^{\mathrm{T}}\mathbf{v}}{H_i} & \text{for } i = 2 \\ (\mathbf{a}(t, \mathbf{d})_i^{\mathrm{T}} - \mathbf{a}(t, \mathbf{d})_{i-1}^{\mathrm{T}})\dfrac{\mathbf{v}}{H_i} & \text{for } i = 3, 4, \ldots, n_s \end{cases} \tag{29}$$

where Δ_i denotes the story drift at floor level i, H_i represents the story height below level i, and n_s is the number of story levels. The instantaneous failure probability in terms of the inter story-drift ratios is

$$\begin{aligned} P(E_{f_{\Delta_i}}(t_k, \mathbf{d})) &= P(g_{\Delta_i}(t_k, \mathbf{d}) \leqslant 0) = P\left(u_{0\Delta_i} - \frac{\Delta_i(t_k, \mathbf{d})}{H_i} \leqslant 0\right) \\ &= \Phi[-\beta_{\Delta_i}(t_k, \mathbf{d})], \quad i = 1, \ldots, n_s \end{aligned} \tag{30}$$

where $u_{0\Delta i}$ denotes a threshold value of the inter-story drift ratio, and $\beta_{\Delta i}$ represents the reliability index which can be computed as

$$\beta_{\Delta i}(t_k, \mathbf{d}) = \begin{cases} \dfrac{H_i u_{0\Delta i}}{\|\mathbf{a}(t_k, \mathbf{d})_i^{\mathrm{T}}\|} & \text{for } i = 2 \\ \dfrac{H_i u_{0\Delta i}}{\|\mathbf{a}(t_k, \mathbf{d})_i^{\mathrm{T}} - \mathbf{a}(t_k, \mathbf{d})_{i-1}^{\mathrm{T}}\|} & \text{for } i = 3, 4, \ldots, n_s \end{cases} \tag{31}$$

Finally, the first-passage probability is

$$\begin{aligned} P_{fp\_\Delta_i}(E_{sys}) &= P\left(\bigcup_{k=1}^{n} E_{f_{\Delta_i}}(t_k, \mathbf{d})\right) = P\left(\bigcup_{k=1}^{n}\left\{u_{0\Delta_i} - \frac{\Delta_i(t_k, \mathbf{d})}{H_i} \leqslant 0\right\}\right) \\ &= 1 - \Phi_n[\beta_{\Delta_i}(t_1, \mathbf{d}), \beta_{\Delta_i}(t_2, \mathbf{d}), \ldots, \beta_{\Delta_i}(t_n, \mathbf{d}); \rho_{1,2}, \rho_{1,3}, \ldots, \rho_{n-1,n}] \\ &= 1 - \Phi_n[\boldsymbol{\beta}_{\Delta_i}, \mathbf{R}] \end{aligned} \tag{32}$$

4. Calculating sensitivity of rst-passage probability

To use efficient gradient-based optimization algorithms for RBDO, it is essential to calculate the sensitivity of the failure probability with respect to various design parameters. In this paper, a sensitivity formulation employing the adjoint method [34] is derived for the first-passage probability of a linear structure based on the discrete

Table 1
Topology optimization problem (Fig. 2): filtering parameters for ground excitations and a threshold value of the probabilistic constraint.

Φ_0	ω_f	ζ_f	t (s)	Δt (s)	$u_{0\Delta}$
100	5π	0.4	5	0.1	1/400

representation method. It is noted that the sensitivity of the system failure probability with respect to a parameter θ is obtained by a chain rule, i.e.

$$\frac{\partial P_f(E_{sys})}{\partial \theta} = \sum_{i=1}^{n} \frac{\partial P_f(E_{sys})}{\partial \beta_i(\theta)} \cdot \frac{\partial \beta_i(\theta)}{\partial \theta} \tag{33}$$

Recently, Chun et al. [25] proposed the CSP method to compute the derivatives of the system failure probability with respect to the reliability index based on the use of the SCM. The CSP method computes sensitivities of parallel and series systems, as well as general systems with respect to reliability indices efficiently and accurately.

4.1. Sensitivity of system reliability using SCM

The CSP method computes parametric sensitivity of the system reliability based on the SCM method. The main idea of the CSP method is carrying out sensitivity analysis after the system failure event is simplified using the SCM. This idea is briefly explained using a series system example formulated as an n-fold integral in the correlated standard normal space, i.e.

$$P(E_{series}) = P(E_1 \bigcup E_2 \bigcup \cdots \bigcup E_n) = P\left[\bigcup_{j=1}^{n} (\beta_j \leqslant Z_j)\right] = \int_{\Omega_f} \varphi_n(\mathbf{z};\mathbf{R})\, d\mathbf{z} \tag{34}$$

Suppose the k-th component is compounded at the last step, i.e. compounded with the super-component E_{S_k}, which denotes the union of all the component events except the k-th one. Utilizing the formula for bi-variate normal CDF [35], the sensitivity of the series system failure probability with respect to β_k is obtained as [25]

$$\frac{\partial P(E_{series})}{\partial \beta_k} = -\varphi(-\beta_k) - \frac{\partial \Phi_2[-\beta_k, -\beta_{S_k}; \rho_{k,S_k}]}{\partial \beta_k} \tag{35}$$

where ρ_{k,S_k} is the updated correlation coefficient between E_k and E_{S_k} obtained during the sequential compounding [24], and

$$\beta_{S_k} = -\Phi[P(E_{S_k})]^{-1} = -\Phi[P(\bigcup_{p \in S_k} E_p)]^{-1} \tag{36}$$

where S_k denotes the index set of the components in E_{S_k}. Similarly, the parameter sensitivities of parallel and cut-set systems were derived by Chun et al. [25].

4.2. Sensitivity of first-passage probability in RBDO

To facilitate the use of a gradient-based optimizer, the sensitivity of the first-passage probability in RBDO is computed using the chain rule, i.e.

$$\frac{\partial P_{fp}(E_{sys})}{\partial d_i} = \frac{\partial (1-\Phi_n[\boldsymbol{\beta}, \mathbf{R}])}{\partial d_i} = \sum_{j=1}^{n} \left(\frac{\partial (-\Phi_n[\boldsymbol{\beta}, \mathbf{R}])}{\partial \beta_j} \cdot \frac{\partial \beta_j(\mathbf{d})}{\partial d_i} \right) = \sum_{j=1}^{n} \left(c_j \cdot \frac{\partial \beta_j(\mathbf{d})}{\partial d_i} \right) \tag{37}$$

where $c_j = (-\Phi[\,, \mathbf{R}])/\beta_j$ can be computed using Eq. (35). The partial derivative $\partial\beta_j/d_i$ is obtained by

$$\frac{\partial \beta_j(\mathbf{d})}{\partial d_i} = -\frac{C_{cst} \cdot \left(\sum_{k=1}^{j} \left(a_k(t_j, \mathbf{d}) \cdot \frac{\partial a_k(t_j, \mathbf{d})}{\partial d_i} \right) \right)}{\left(\sum_{k=1}^{j} a_k(t_j, \mathbf{d})^2 \right)^{3/2}} \tag{38}$$

where C_{cst} is the coefficient determined depending on the constraint used in optimization, e.g.

$$C_{cst} = \begin{cases} L_e \sigma_{0e}/D_e & : \text{stress in bar} \\ H u_{0\Delta} & : \text{drift ratio} \\ H_i u_{0\Delta_i} & : \text{inter-story drift ratio} \end{cases} \tag{39}$$

When a uniform time step size is used, i.e. $t_i - t_{i-1} = \Delta t,\ i = 1, 2, \ldots, n$ and $t_n = t_0$, Eq. (38) can be rewritten from Eq. (4) as follows (see more details of the derivation in Appendix of Chun et al. [14]):

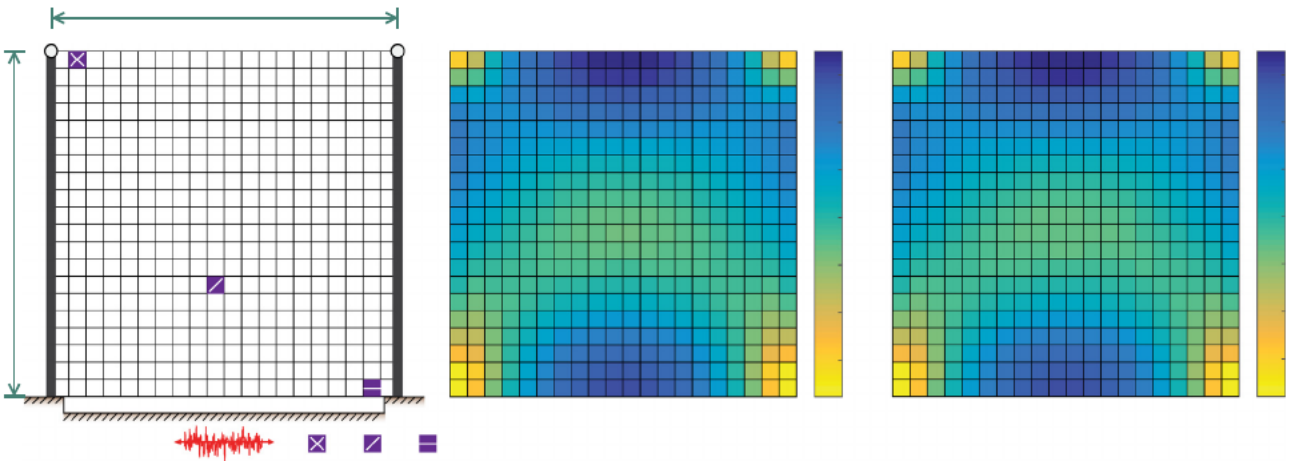

Fig. 2. Sensitivity comparison: (a) geometry, loading condition, and locations where sensitivity is reported (Table 2), (b) sensitivities from the adjoint method (AJM), and (c) sensitivities from the finite difference method (FDM).

Table 2
Sensitivity comparison of first-passage probability on a displacement constraint in topology optimization.

Δd	FDM			AJM		
	$\partial P_f/\partial d_A$	$\partial P_f/\partial d_B$	$\partial P_f/\partial d_C$	$\partial P_f/\partial d_A$	$\partial P_f/\partial d_B$	$\partial P_f/\partial d_C$
1×10^{1}	−0.000452	−0.000293	−0.000569	−0.000486	−0.000312	−0.000599
1×10^{-2}	−0.000483	−0.000310	−0.000596			
1×10^{-3}	−0.000486	−0.000312	−0.000599			
1×10^{-4}	−0.000487	−0.000312	−0.000599			
1×10^{-5}	−0.000487	−0.000312	−0.000599			
1×10^{-6}	−0.000486	−0.000312	−0.000599			
1×10^{-7}	−0.000485	−0.000309	−0.000598			
1×10^{-8}	−0.000479	−0.000301	−0.000619			
1×10^{-9}	−0.000444	−0.000391	−0.000632			
1×10^{-10}	0.000250	0.000289	−0.000012			
1×10^{-11}	−0.000166	−0.001532	−0.004141			
1×10^{-12}	0.050625	0.025424	0.036526			

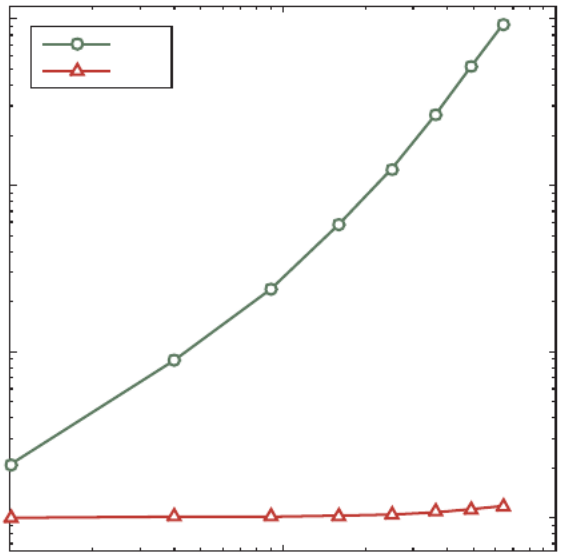

Fig. 3. Computational time comparison for sensitivity analysis by the FDM and the AJM.

$$\frac{\partial \beta_j(\mathbf{d})}{\partial d_i} = -\frac{C_{cst}\cdot\left(\sum_{k=n-j+1}^{n}\left(a_k(t_n,\mathbf{d})\cdot\frac{\partial a_k(t_n,\mathbf{d})}{\partial d_i}\right)\right)}{\left(\sum_{k=n-j+1}^{n} a_k(t_n,\mathbf{d})^2\right)^{3/2}} \tag{40}$$

Furthermore, the uniform step size leads to the followings for the parameter sensitivity in Eq. (37):

$$\frac{\partial P_{fp}(E_{sys})}{\partial d_i} = \sum_{j=1}^{n}\left(c_j\cdot\frac{\partial \beta_j(\mathbf{d})}{\partial d_i}\right) = \left(C_{cst}\cdot\sum_{l=1}^{n}\left(\chi_l\, a_{n-l+1}(t_n,\mathbf{d})\frac{\partial a_{n-l+1}(t_n,\mathbf{d})}{\partial d_i}\right)\right) = \sum_{s=1}^{n}\left(\kappa_s(t_n,\mathbf{d})\frac{\partial a_s(t_n,\mathbf{d})}{\partial d_i}\right) \tag{41}$$

where

$$\chi_l = -\sum_{i=l}^{n}\left(c_i/\left(\sum_{k=n-i+1}^{n} a_k(t_n,\mathbf{d})^2\right)^{3/2}\right), \quad \kappa_s(t_n,\mathbf{d}) = C_{cst}\chi_{n-s+1}\cdot a_s(t_n,\mathbf{d}) \tag{42}$$

4.3. Sensitivity of first-passage probability by adjoint variable method

The sensitivity in Eq. (41) includes the implicitly defined derivative term of $\partial a_s(t_n,\mathbf{d})/\partial d_i$, $s = 1,\ldots, n$. Those implicit derivatives can be computed using the direct differentiation method (DDM), the finite difference method (FDM) or the adjoint variable method (AJM) [34].

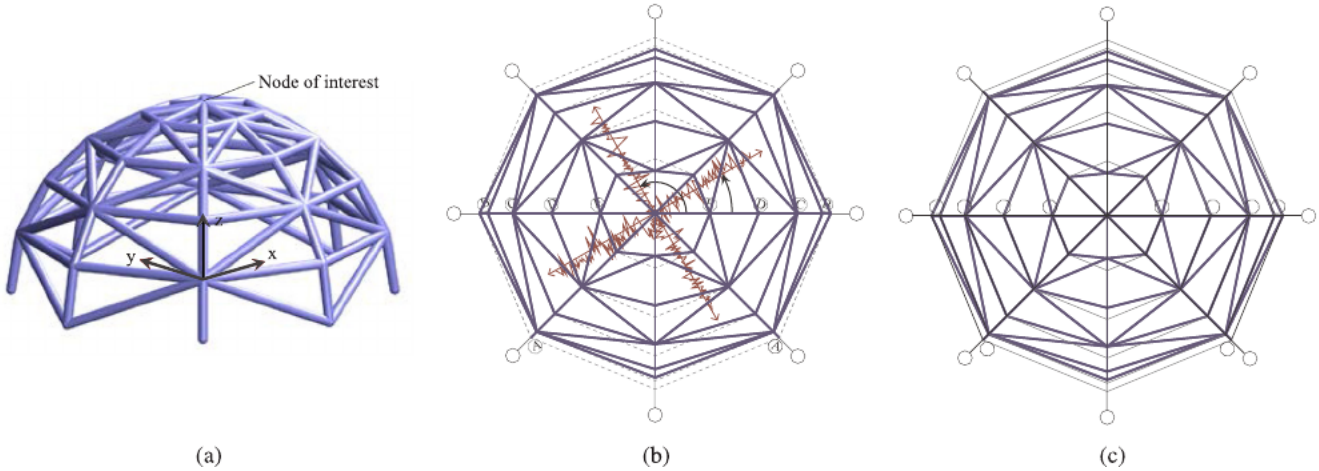

Fig. 4. A space truss dome example: (a) perspective view of the dome, (b) plan view and directions of applied ground accelerations and (c) element numbering choices.

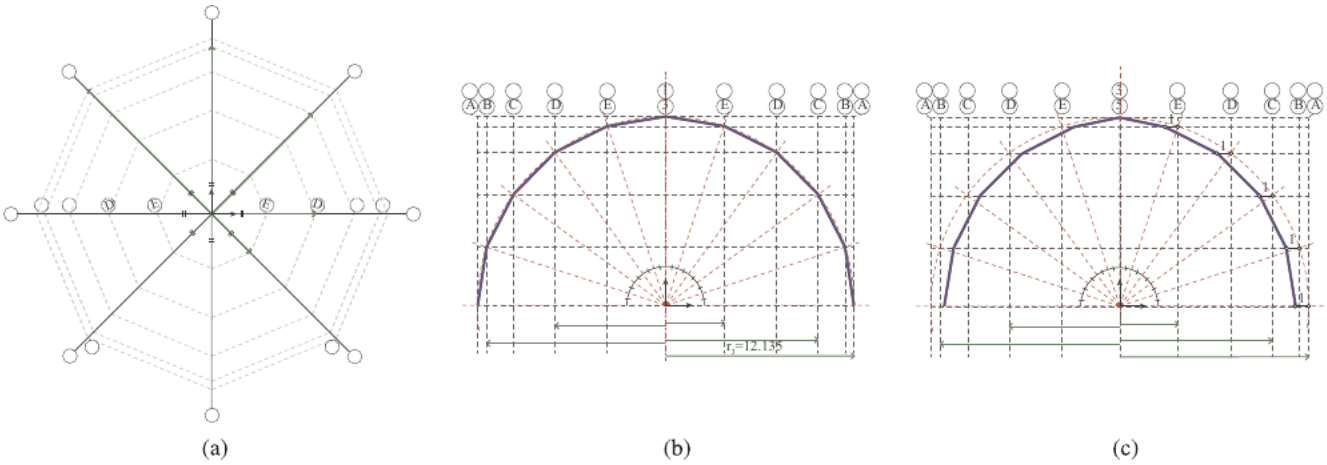

Fig. 5. Geometry of a space truss dome: (a) basic grid, (b) section view along grid line 1–5, and (c) section view along grid line 3–7.

Table 3
Parameters for filters of ground motion models and constraints in optimization (space truss dome optimization example).

Φ_{0_g1}	Φ_{0_g2}	ω_f	ζ_f	t (s)	Δt (s)	Initial cross-section areas (m^2)	Threshold value
4.0	3.0	5π	0.4	6.0	0.06	0.25	$u_{0\Delta x} = 1/800$ $u_{0\Delta y} = 1/800$

Chun et al. [14] derived an approach of sensitivity calculations associated with $\partial a_s(t_n, \mathbf{d})/\partial d_i$ using the adjoint variable method. The numerical tests confirmed superior performance of AJM compared to DDM and FDM. Based on the AJM derivation, the sensitivity of the first-passage probability in Eq. (41) is rewritten as

$$\begin{aligned}\frac{\partial P_{fp}(E_{sys})}{\partial d_i} = \sum_{j=1}^{n} \boldsymbol{\lambda}_{n-j+1}^{\mathrm{T}} \Bigg[& \frac{\partial \underline{\underline{\mathbf{A}}}(\mathbf{d})}{\partial d_i}\cdot\mathbf{u}(t_j,\mathbf{d}) - \eta(\Delta t)^2\frac{\partial \mathbf{f}(t_j,\mathbf{d})}{\partial d_i} \\ & -(0.5+\gamma-2\eta)(\Delta t)^2\frac{\partial \mathbf{f}(t_{j-1},\mathbf{d})}{\partial d_i} - (0.5-\gamma+\eta)(\Delta t)^2\frac{\partial \mathbf{f}(t_{j-2},\mathbf{d})}{\partial d_i} \\ & + \frac{\partial \underline{\underline{\mathbf{B}}}(\mathbf{d})}{\partial d_i}\cdot\mathbf{u}(t_{j-1},\mathbf{d}) + \frac{\partial \underline{\underline{\mathbf{E}}}(\mathbf{d})}{\partial d_i}\cdot\mathbf{u}(t_{j-2},\mathbf{d}) \Bigg] \\ & + \boldsymbol{\lambda}_n^{\mathrm{T}}\left[\underline{\underline{\mathbf{B}}}(\mathbf{d})\cdot\frac{\partial \mathbf{u}(0,\mathbf{d})}{\partial d_i} + \underline{\underline{\mathbf{E}}}(\mathbf{d})\cdot\frac{\partial \mathbf{u}(t_{-1},\mathbf{d})}{\partial d_i}\right] \\ & + \boldsymbol{\lambda}_{n-1}^{\mathrm{T}}\left[\underline{\underline{\mathbf{E}}}(\mathbf{d})\cdot\frac{\partial \mathbf{u}(0,\mathbf{d})}{\partial d_i}\right]\end{aligned} \tag{43}$$

where $\boldsymbol{\lambda}_{n-j+1}$ denotes the adjoint variable vector. $\underline{\underline{\mathbf{A}}}(\mathbf{d})$, $\underline{\underline{\mathbf{B}}}(\mathbf{d})$, and $\underline{\underline{\mathbf{E}}}(\mathbf{d})$ represent followings respectively:

$$\begin{aligned}\underline{\underline{\mathbf{A}}}(\mathbf{d}) &= \mathbf{M}(\mathbf{d}) + \gamma\Delta t\cdot\mathbf{C}(\mathbf{d}) + \eta(\Delta t)^2\mathbf{K}(\mathbf{d}) \\ \underline{\underline{\mathbf{B}}}(\mathbf{d}) &= -2\mathbf{M}(\mathbf{d}) + (1-2\gamma)\Delta t\mathbf{C}(\mathbf{d}) + (0.5+\gamma-2\eta)(\Delta t)^2\mathbf{K}(\mathbf{d}) \\ \underline{\underline{\mathbf{E}}}(\mathbf{d}) &= \mathbf{M}(\mathbf{d}) + (\gamma-1)\Delta t\mathbf{C}(\mathbf{d}) + (0.5-\gamma+\eta)(\Delta t)^2\mathbf{K}(\mathbf{d})\end{aligned} \tag{44}$$

4.4. Sensitivity analysis of first-passage probability in RBTO

Sensitivity analysis of first-passage probability in stochastic *topology* optimization is similar to the derivation for RBDO described above. The main difference of sensitivity analysis in topology optimization comes from the projection method to obtain the filtered density as shown below.

$$\begin{aligned}\frac{\partial P_{fp}(E_{sys})}{\partial d_i} &= \frac{\partial(1-\Phi_n[\boldsymbol{\beta},\mathbf{R}])}{\partial d_i} = \sum_{j=1}^{n}\left(\frac{\partial(-\Phi_n[\boldsymbol{\beta},\mathbf{R}])}{\partial\beta_j}\cdot\frac{\partial\beta_j(\tilde{\boldsymbol{\rho}})}{\partial d_i}\right) \\ &= \sum_{j=1}^{n}\left(\frac{\partial(-\Phi_n[\boldsymbol{\beta},\mathbf{R}])}{\partial\beta_j}\cdot\sum_{l=1}^{n_e}\left(\frac{\partial\beta_j(\tilde{\boldsymbol{\rho}})}{\partial\tilde{\rho}_l}\cdot\frac{\partial\tilde{\rho}_l}{\partial d_i}\right)\right) \\ &= \sum_{j=1}^{n}\left(\frac{\partial(-\Phi_n[\boldsymbol{\beta},\mathbf{R}])}{\partial\beta_j}\cdot\left((\mathbf{P})_{i^{\mathrm{th}}\,\mathrm{row}}^{\mathrm{T}}\cdot\frac{\partial\beta_j(\tilde{\boldsymbol{\rho}})}{\partial\tilde{\boldsymbol{\rho}}}\right)\right) \\ &= (\mathbf{P})_{i^{\mathrm{th}}\,\mathrm{row}}^{\mathrm{T}}\cdot\sum_{j=1}^{n}\left(\frac{\partial(-\Phi_n[\boldsymbol{\beta},\mathbf{R}])}{\partial\beta_j}\cdot\frac{\partial\beta_j(\tilde{\boldsymbol{\rho}})}{\partial\tilde{\boldsymbol{\rho}}}\right)\end{aligned} \tag{45}$$

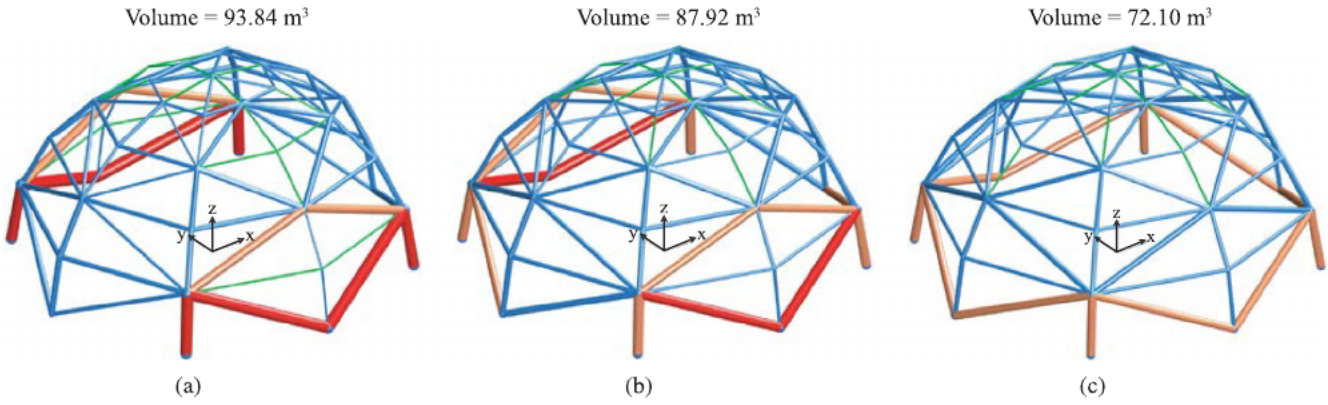

Fig. 6. Optimized space truss dome corresponding to different angles of ground accelerations: (a) $\theta_{g1} = 0^\circ$, $\theta_{g2} = 30^\circ$, (b) $\theta_{g1} = 0^\circ$, $\theta_{g2} = 60^\circ$, (c) $\theta_{g1} = 0^\circ$, $\theta_{g2} = 90^\circ$ (Color legends: $A_i = A_{min}$ in green, $0.02\,m^2 < A_i \le 0.2\,m^2$ in blue, $0.2\,m^2 < A_i \le 0.4\,m^2$ in brown, $0.4\,m^2 < A$ in red). (For interpretation of the references to color in this figure legend, the reader is referred to the web version of this article.)

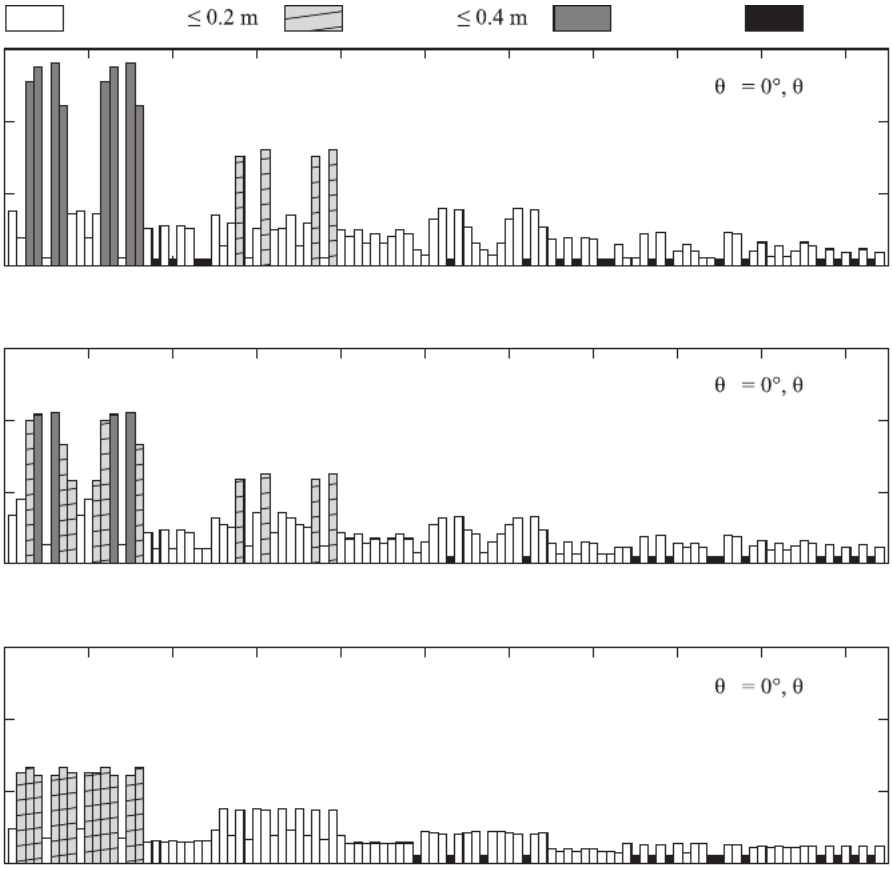

Fig. 7. Optimized cross-sectional areas of truss elements corresponding to the ground accelerations applied at different angles.

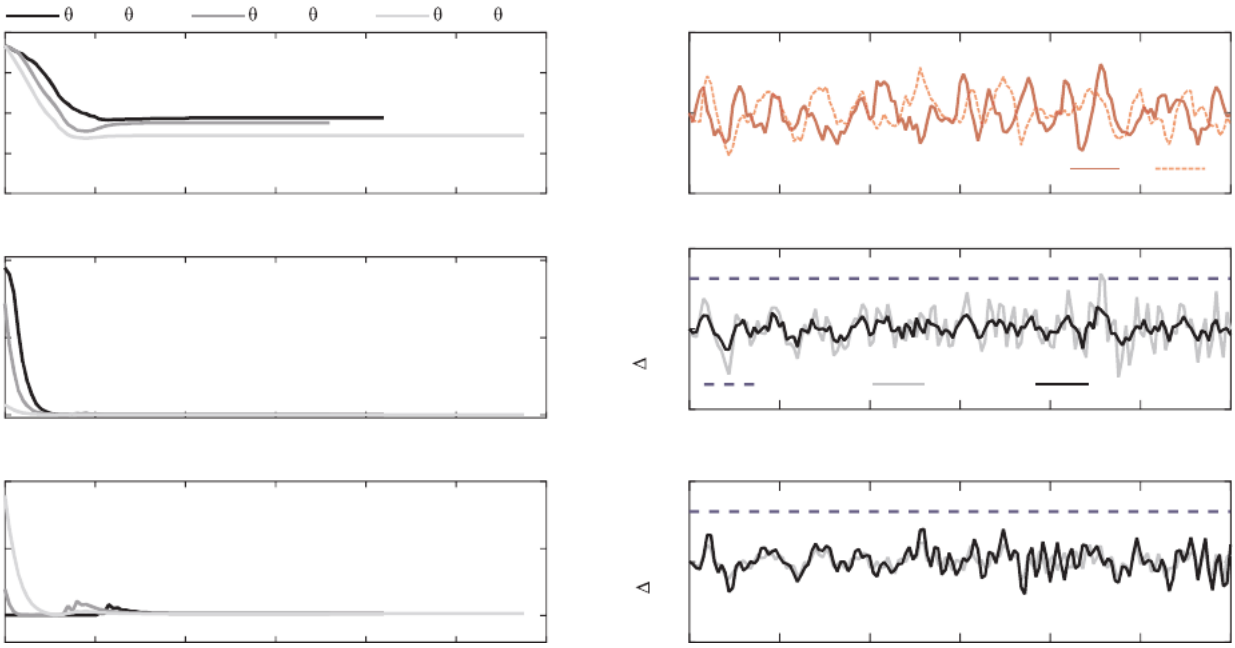

Fig. 8. Convergence history: (a) volume and (b) first-passage probability. Comparison between dynamic responses by the initial structure and the optimized structures: (c) randomly generated ground accelerations ($\theta_{g1} = 0^{\circ}$, $\theta_{g2} = 30^{\circ}$), (d) drift ratio in the *x*-direction and (e) drift ratio in the *y*-direction.

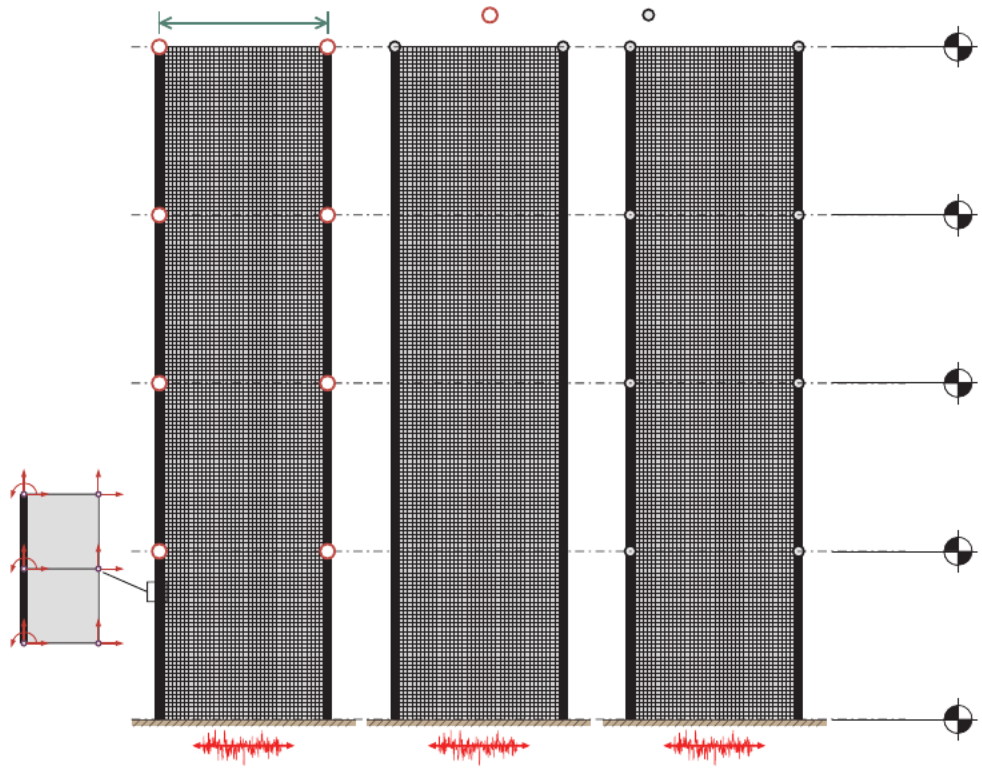

Fig. 9. (a) Design domain and loading condition, (b) node of interest for a tip drift ratio constraint, and (c) nodes of interest for inter-story drift ratios.

Table 4
Parameters for ground motion filter model and constraints of topology optimization (topology optimization example).

Φ_0	ω_f	ζ_f	t (s)	Δt (s)	Init. density	Colum size	Thres. value
7.5	5π	0.4	6.0	0.06	0.7	0.6 m × 0.6 m	$u_{0\Delta} = 1/50$

where $\mathbf{P}^{\mathrm{T}}$ denotes the transpose of the filtering matrix in Eq. (19) and $(\mathbf{P})^{\mathrm{T}}_{i^{\mathrm{th}}\,\mathrm{row}}$ is the i-th row vector of P^{T}. Thus,

$$\frac{\partial P_{fp}(E_{sys})}{\partial \mathbf{d}} = \mathbf{P}^{\mathrm{T}} \sum_{j=1}^{n} \left(\frac{\partial(-\Phi_n[\boldsymbol{\beta}, \mathbf{R}])}{\partial \beta_j} \cdot \frac{\partial \beta_j(\tilde{\boldsymbol{\rho}})}{\partial \tilde{\boldsymbol{\rho}}} \right) \tag{46}$$

where the partial derivative of $\beta_j(\cdot)$ with respect to an element density can be computed as explained in Sections 4.2 and 4.3.

4.5. Veri cation of calculated sensitivity

The adjoint sensitivity method derived for the first-passage probability constraints is tested for the topology optimization problem in Fig. 2(a) through comparison with the finite difference method to verify accuracy and efficiency. The stochastic seismic acceleration $f(t)$ is modeled as a filtered white-noise process using the Kanai-Tajimi filter model with the intensity Φ_0 [26,23]. The unit-impulse response function of the filter and the effective force vector caused by the earthquake excitation are determined as follows, respectively:

$$h_f^{\mathrm{KT}}(t) = \exp(-\zeta_f \omega_f t) \left[\frac{(2\zeta_f^2 - 1)\omega_f}{\sqrt{1-\zeta_f^2}} \sin(\omega_f \sqrt{1-\zeta_f^2} \cdot t) - 2\zeta_f \omega_f \cos(\omega_f \sqrt{1-\zeta_f^2} \cdot t) \right] \tag{47}$$

$$\mathbf{f}(\mathbf{d}, t) = -\mathbf{M}(\mathbf{d})\mathbf{l} f(t) = -\mathbf{M}(\mathbf{d})\mathbf{l} \cdot \left(\int_0^t h_f^{\mathrm{KT}}(t-\tau) W(\tau) d\tau \right) \tag{48}$$

Table 1 summarizes the Kanai-Tajimi filter parameters of dominant frequency ω_f and bandwidth ζ_f, the time interval of interest, and the threshold value of the drift ratio at each time point.

The sensitivities of the first-passage probability with respect to the design variables located at the three points A, B and C in Fig. 2(a) are computed by the proposed adjoint method and the FDM, respectively. The structural columns represented by two vertical lines in Fig. 2(a) are modeled by frame elements. Young's modulus $E = 21{,}000$ MPa and mass density $\rho_m = 2{,}400\ \mathrm{kg/m}^3$ are used as material properties for both the quadrilateral and frame elements. The instantaneous failure event at a discretized time point is considered in terms of an averaged drift ratio evaluated at two nodes of interest. Thus, the first-passage event is defined as

$$E_{sys} = \bigcup_{k=1}^{n} E_{f_{\Delta i}}(t_k, \tilde{\boldsymbol{\rho}}) = \bigcup_{k=1}^{n} \left(u_{0\Delta} - \frac{(\mathbf{a}(t_k, \tilde{\boldsymbol{\rho}})^{\mathrm{T}}_{Left} + \mathbf{a}(t_k, \tilde{\boldsymbol{\rho}})^{\mathrm{T}}_{Right})\mathbf{v}}{2H} \leqslant 0 \right) \tag{49}$$

The sensitivities of the first-passage probability constraint in Eq. (49) are shown in Fig. 2(b) and (c), which show good agreements. The sensitivities by the FDM employing a range of perturbations (from 10^{-1} to 10^{-12}) are tabulated in Table 2 for comparison with the results by the AJM, and the influence of the perturbation size on the results by the

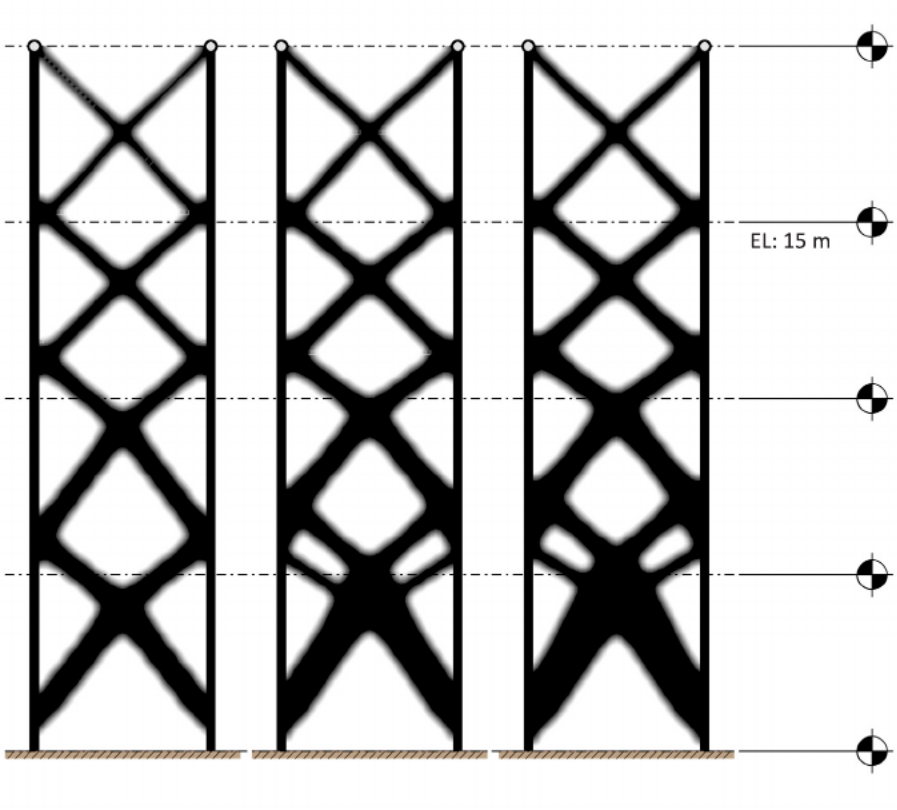

Fig. 10. Topology optimization results from the four-story building example constrained by the first-passage probability in term of the tip drift ratio constraint: (a) $\beta^{target} = 1.5$, $P_f^{target} = 6.68\%$, (b) $\beta^{target} = 2.5$, $P_f^{target} = 0.62\%$, and (c) $\beta^{target} = 3.0$, $P_f^{target} = 0.13\%$.

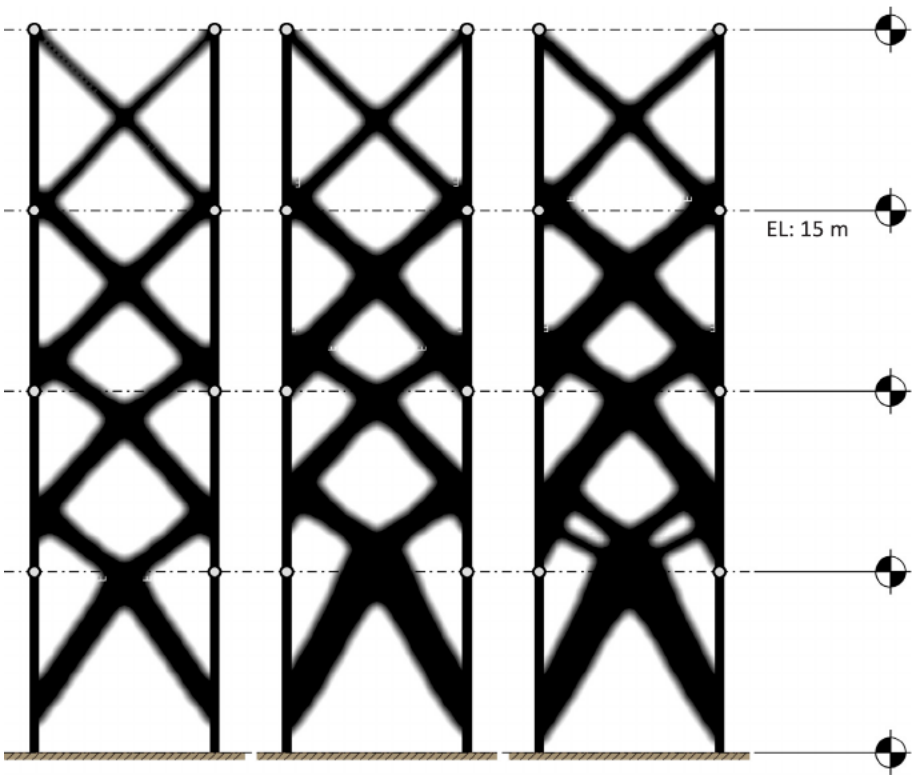

Fig. 11. Topology optimization results from the four-story building example constrained by the first-passage probabilities in terms of inter-story drift ratio: (a) $\beta^{target} = 1.5$, $P_f^{target} = 6.68\%$, (b) $\beta^{target} = 2.5$, $P_f^{target} = 0.62\%$, and (c) $\beta^{target} = 3.0$, $P_f^{target} = 0.13\%$.

FDM. The computational costs of the two methods are compared in Fig. 3 while varying the number of elements in the problem. The computational costs are normalized by that of the AJM for the 100-element case. It is noted that the proposed AJM requires dramatically less computational time than the FDM. It should also be noted that unlike FDM, AJM does not require determining the perturbation size, for which an optimal choice is generally not known a priori.

5. Numerical applications

5.1. Space truss dome optimization

In this example, the weight of an asymmetric space truss dome composed of 104 elements (Fig. 4) is minimized under constraints on the first-passage probability of the drift ratio evaluated at the node of interest, i.e. the highest elevation. The basic grid of the structure, plan view, and section views are provided in Fig. 5. Fig. 4(c) shows the element numbering choices of the space truss dome. At each node of the structure, additional masses (10,000 kg) representing non-structural masses such as claddings are equally applied. Young's modulus $E = 210$ GPa and mass density $_m = 7{,}850$ kg are used as material properties for each truss element. The ground acceleration is generated by using the Kanai-Tajimi filter. The filter and optimization parameters are presented in Table 3. The probabilistic constraint is defined in terms of the tip drift ratio evaluated at the top ($z = 15$ m). For a loading scenario, two direction components of earthquake ground excitations at angles (θ_{g1}, θ_{g2}) shown in Fig. 4(b) are considered simultaneously and applied to the structure. The target failure probability and a lower bound of design variables are set to $P_f^{\text{target}} = 0.0013$ ($\beta_f^{\text{target}} = -\Phi[P_f^{\text{target}}]^{-1} = 3.0$) and $0.02\,\text{m}^2$. The optimization formulation considering multiple ground accelerations with constraints on drift ratios in both x- and y-directions is developed as

$$
\begin{aligned}
&\min_{\mathbf{d}} \quad f_{obj}(\mathbf{d}) \\
&\text{s. t} \quad P_{fp,x-dir}\left(\bigcup_{k=1}^{n}\left(E_{f_x}(t_k,\mathbf{d}): g_x(t_k,\mathbf{d}) \leqslant 0\right)\right) \leqslant P_{f_x-\text{dir}}^{\text{target}} \\
&\qquad P_{fp,y-dir}\left(\bigcup_{k=1}^{n}\left(E_{f_y}(t_k,\mathbf{d}): g_y(t_k,\mathbf{d}) \leqslant 0\right)\right) \leqslant P_{f_y-\text{dir}}^{\text{target}} \\
&\qquad 0.02\text{m}^2 \leqslant \mathbf{d} \leqslant 1.5\text{m}^2 \\
&\text{with} \quad \mathbf{M}(\mathbf{d})\ddot{\mathbf{u}}(t,\mathbf{d}) + \mathbf{C}(\mathbf{d})\dot{\mathbf{u}}(t,\mathbf{d}) + \mathbf{K}(\mathbf{d})\mathbf{u}(t,\mathbf{d}) = -\mathbf{M}(\mathbf{d})\mathbf{l}(\theta_{g1})f_{g1}(t) \\
&\qquad\qquad -\mathbf{M}(\mathbf{d})\mathbf{l}(\theta_{g2})f_{g2}(t)
\end{aligned}
\tag{50}
$$

Fig. 6 shows that the space truss domes optimized with fixed θ_{g1} while varying θ_{g2} to three different angles. Optimal results from the case of the applied ground acceleration with $\theta_{g1} = 0^\circ$, $\theta_{g2} = 90^\circ$ show

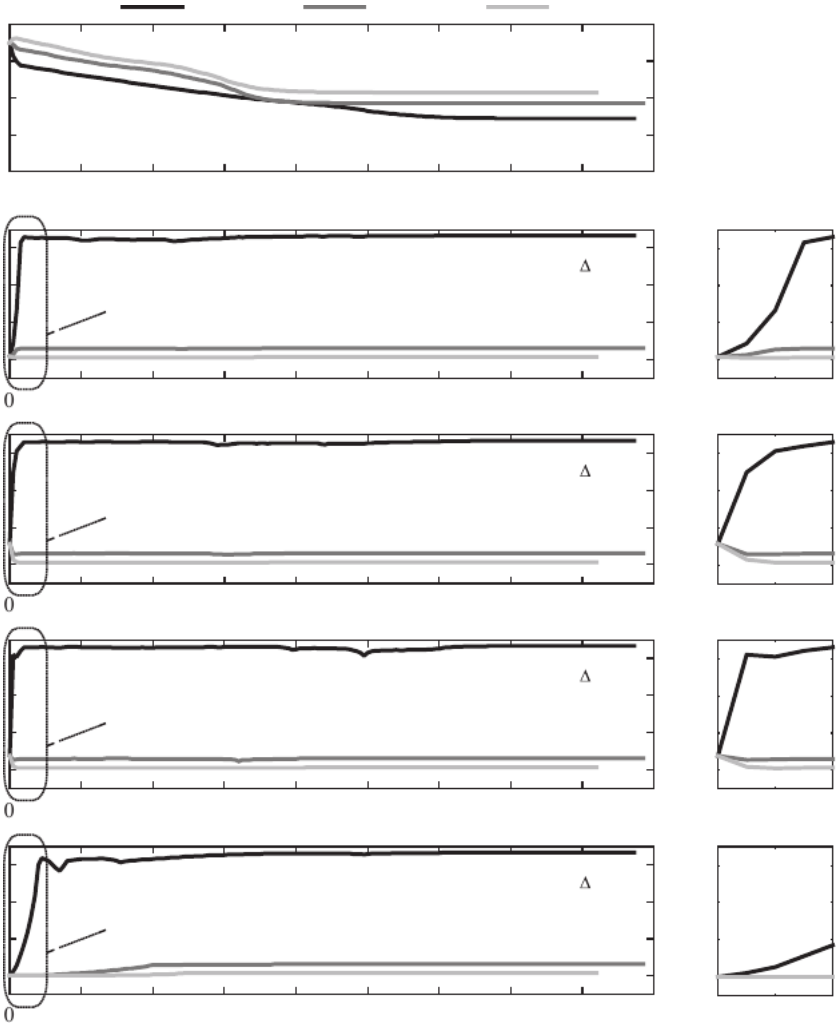

Fig. 12. Convergence history of the four-story building. First-passage probabilities of inter-story drift ratio constraints: (a) volume and (b) first-passage probability of each inter-story drift ratio.

that the cross-sectional areas of bracings and vertical elements, especially at a lower level, are increased to reduce displacements in both *x*- and *y*-directions and failure probabilities. Also, as the angle θ_{g2} becomes closer to θ_{g1}, the optimal volume increases. By changing θ_{g2} from 90° to 60° (or 30°), the increase in the failure probability in the x-direction is much higher than the decrease in the failure probability in the y-direction. The optimized area of each element is plotted in Fig. 7. As expected, truss members, which are closely aligned to the applied ground accelerations are enlarged especially for lower levels. Thus, truss members are sized more symmetrically in both x- and y- directions for ground accelerations with $\theta_{g1} = 0°$, $\theta_{g2} = 90°$ compared to $\theta_{g2} = 30°$ or $\theta_{g2} = 60°$. Fig. 8(a) and (b) show convergence histories of the volume and the first-passage probability. The proposed method enables achieving the target failure probability with reduced volumes. The comparison of dynamic responses of the initial structure and the optimized structure is shown in Fig. 8(c) through (e) under randomly generated samples of ground excitations with the filter parameters reported in Table 3. Overall reductions in the drift ratio in the optimized structure are observed, which naturally reduces the likelihood of exceedance of the threshold value during the excitation.

5.2. Optimization of a bracing system using topology optimization

The previous numerical application of the bracing system is considered as *size* optimization for a given structural layout. By contrast, *topology* optimization can identify the optimal bracing layout of a structure. To demonstrate this optimization under first-passage probability constraints, the proposed method is applied to the design domain under earthquake excitations as shown in Fig. 9(a). During the optimization for minimizing volume, the first-passage failures are defined in terms of inter-story drift ratios at each level, and a tip drift ratio at the building height (see Fig. 9(b) and (c)). The structural columns represented by two vertical lines shown in Fig. 9(a) are modeled by frame elements whose densities remain unchanged throughout the optimization process. Young's modulus $E = 21{,}000\,\text{MPa}$ and mass density $_m = 2{,}400\,\text{kg/m}^3$ are used as material properties for both the quadrilateral and frame elements. The additional mass of 4,000 kg is considered at each floor level as shown in Fig. 9(a). The damping matrix is constructed using a Rayleigh damping model with a 2% damping ratio.

Table 4 summarizes the Kanai-Tajimi filter parameters of dominant frequency ω_f and bandwidth ζ_f, column size, the time interval of interest, and the threshold value u_0 of the average drift ratio at each time point. The filtering radius r is 0.25 m, and a prescribed density 0.7 is applied uniformly throughout the mesh. Topology optimization results are shown from different target failure probabilities of the inter-story drift ratios, and the tip-drift ratio constraints are shown in Figs. 10 and 11. For the tip drift ratio constraint, the increase in the thicknesses in lower levels and additional branches of material distributions are observed as the target failure probabilities decrease, whereas bracing points and topologies remain relatively the same for all three cases under the tip drift ratio constraint in Fig. 10. On the other hand, Fig. 11 shows that connections of topologies to each floor level can be checked for inter-story drift ratio constraints except the lowest level. As the target failure probability is reduced, the second lowest intersection point of bracing and column also decreases in elevation, such that in the case of Fig. 11(c), the intersection point is on the second level. Intersection points of bracings for upper two levels in both constrained optimization problems are at the midpoint of two floors so that X shapes of bracings with 90° are observed. At lower levels, the bracing intersection points become higher. In addition, there is a significant increase in material distribution in lower levels of the tip displacement constraint, whereas overall thicknesses of bracings throughout the building height are increased for the inter-story drift ratio constraint. Thus, optimization results show that reinforcing lower regions will be an efficient approach to control the tip displacement whereas adjusting each bracing module will lead to successful designs of structures fulfilling inter-story drift ratio criteria (see Fig. 12).

For constructability and aesthetic aspect of architecture, a pattern repetition constraint [33,36] can be implemented in the proposed framework. Therefore, different choices regarding the number of patterns or size of the primary region in optimization will result in various topologies, which can provide diverse options of solutions for the architectural and engineering schematic design process.

6. Summary and concluding remarks

In this paper, an optimization framework is proposed to incorporate the first-passage probability into size optimization and topology optimization of structures. Using the discrete representation method and theories of structural system reliability, the first-passage probability is computed efficiently during the optimization process with a proper consideration of the statistical dependence between component failure events.

Parameter sensitivity formulation of the probabilistic constraint on the first-passage probability is also derived based on the adjoint method and sequential compounding method to facilitate the usage of efficient optimization algorithms. The developed method is successfully applied to the lateral bracing system of structures subjected to stochastic ground motions to identify optimal member sizes under engineering constraints associated with structural design criteria such as the stress, the displacement as well as the inter-story drift ratio. In the numerical application of the space truss dome subject to simultaneous multiple earthquake ground motions, the proposed optimization framework provides reliable structural solutions for various loading scenarios.

Furthermore, the proposed method can be further extended to consider the first-passage probability constraint constructed by combining different types of failure events such as different time points and locations as well as multiple design criteria. The optimized system can withstand future realization of stochastic processes with a desired level of reliability. In addition, numerical examples show that the proposed topology optimization framework can provide an efficient way for structural engineers to obtain optimal design solutions that satisfy probabilistic constraints on the stochastic response in the conceptual (and schematic) design process.

The proposed method is based on the assumption of a stationary process for the earthquake ground motions. The stochastic excitation generated by natural hazards (e.g. earthquakes, hurricanes) can be non-stationary and/or non-Gaussian. Thus, future research could focus on developments of optimization frameworks under non-stationary stochastic processes in the time domain as well as in frequency domain.

Acknowledgements

The authors gratefully acknowledge funding provided by the National Science Foundation (NSF) through projects 1234243 and 1663244. The second author acknowledges the support from the Institute of Engineering Research at Seoul National University. The third author acknowledges support from the Raymond Allen Jones Chair at the Georgia Institute of Technology. The information provided in this paper is the sole opinion of the authors and does not necessarily reflect the views of the sponsoring agencies.

Appendix A

Flowchart of implementation for RBTO of structures constrained by first-passage probability.
Fig. A1

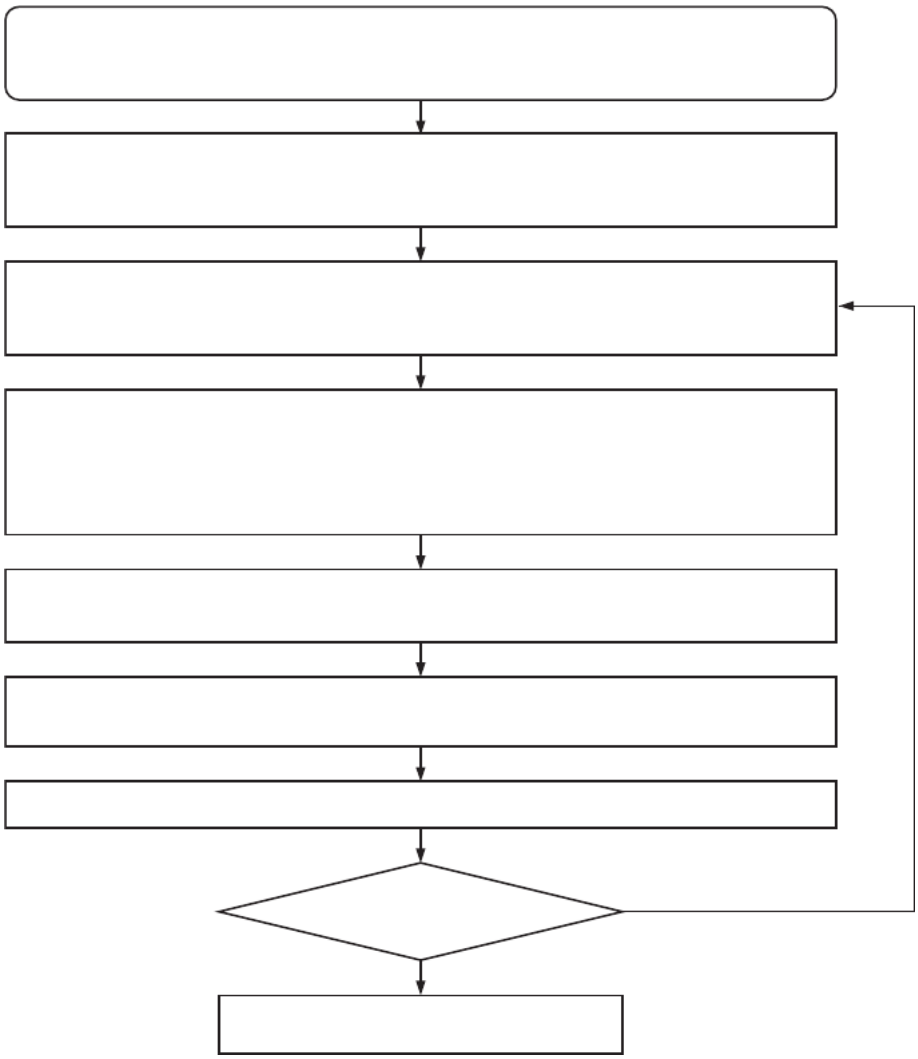

Fig. A1. Flowchart for topology optimization of a structure constrained by first-passage probability.

References

[1] Asadpoure A, Tootkaboni M, Guest J. Robust topology optimization of structures with uncertainties in stiffness—application to truss structures. Comput Struct 2011;89(11–12):1131–41.

[2] Jansen M, Lombaert G, Schevenels M. Robust topology optimization of structures with imperfect geometry based on geometric nonlinear analysis. Comput Methods Appl Mech Eng 2015;285:452–67.

[3] Wang F, Lazarov B, Sigmund O. On projection methods, convergence and robust formulations in topology optimization. Struct Multidiscip Optim 2011;43(6):767–84.

[4] Maute K, Frangopol DM. Reliability-based design of MEMS mechanisms by topology optimization. Comput Struct 2003;81(8–11):813–24.

[5] Frangopol DM, Maute K. Reliability-based optimization of civil and aerospace structural systems. Engineering Design Reliability Handbook. Boca Raton, FL: CRC; 2005. Chap. 24.

[6] Tsompanakis Y, Lagaros ND, Papadrakakis M. Structural Design Optimization Considering Uncertainties. London, UK: Taylor & Francis; 2008.

[7] Guest JK, Igusa T. Structural optimization under uncertain loads and nodal locations. Comput Methods Appl Mech Eng 2008;198(1):116–24.

[8] Rozvany GIN. Exact analytical solutions for benchmark problems in probabilistic topology optimization. In: EngOpt 2008–International Conference on Engineering Optimization, Rio de Janeiro; 2008.

[9] Nguyen TH, Song J, Paulino GH. Single-loop system reliability-based topology optimization considering statistical dependence between limit-states. Struct Multidiscip Optim 2011;44(5):593–611.

[10] Jalalpour M, Guest JK, Igusa T. Reliability-based topology optimization of trusses with stochastic stiffness. Struct Saf 2013;43:41–9.

[11] Salajegheh E, Heidari A. Optimum design of structures against earthquake by wavelet neutral network and filter banks. Earthquake Eng Struct Dyn 2005;34(1):67–82.

[12] Kaveh A, Farzam M, Kalateh M. Time-history analysis based optimal design of space trusses: the CMA evolution strategy approach using GRNN and WA. Struct Eng Mech 2012;44(3):379–403.

[13] Filipov ET, Chun J, Paulino GH, Song J. Polygonal multiresolution topology optimization (PolyMTOP) for structural dynamics. Struct Multidiscip Optim 2016;53(4):673–94.

[14] Chun J, Song J, Paulino GH. Structural topology optimization under constraints on instantaneous failure probability. Struct Multidiscip Optim 2016;53(4):773–99.

[15] Der Kiureghian A. The geometry of random vibrations and solutions by FORM and SORM. Probab Eng Mech 2000;15(1):81–90.

[16] Der Kiureghian A. First- and second-order reliability methods. In: Nikolaidis E, Ghiocel DM, Singhal S, editors. Chapter 14 in Engineering Design Reliability Handbook. Boca Raton, FL: CRC Press; 2005.

[17] Chun J, Song J, Paulino GH. System reliability based topology optimization of structures under stochastic excitations. In: 11th International Conference on Structural Safety & Reliability, New York, NY; 2013.
[18] Song J, Kang WH. System reliability and sensitivity under statistical dependence by matrix-based system reliability method. Struct Saf 2009;31(2):148–56.
[19] Spence SMJ, Gioffre M, Kareem A. An efficient framework for the reliability-based design optimization of large-scale uncertain and stochastic linear systems. Probab Eng Mech 2016;44:174–82.
[20] Bobby S, Spence SMJ, Kareem A. Data-driven performance-based topology optimization of uncertain wind-excited tall buildings. Struct Multidiscip Optim 2016;54:1379–402.
[21] Vanmarcke EH. On the distribution of the first-passage time for normal stationary random processes. J Appl Mech 1975;42(1):215–20.
[22] Song J, Der Kiureghian A. Joint first-passage probability and reliability of systems under stochastic excitation. J Eng Mech 2006;132(1):65–77.
[23] Fujimura K, Der Kiureghian A. Tail-equivalent linearization method for nonlinear random vibration. Probab Eng Mech 2007;22(1):63–76.
[24] Kang WH, Song J. Evaluation of multivariate normal integrals for general systems by sequential compounding. Struct Saf 2010;32(1):35–41.
[25] Chun J, Song J, Paulino GH. Parameter sensitivity of system reliability using sequential compounding method. Struct Saf 2015;55:26–36.
[26] Clough R, Penzien J. Dynamics of Structures. New York: McGraw Hill; 1993.
[27] Bendsøe MP, Sigmund O. Topology Optimization – Theory, Methods and Applications. second ed. Berlin, Germany: Engineering Online Library. Springer; 2003.
[28] Bendsøe MP, Sigmund O. Material interpolation schemes in topology optimization. Arch Appl Mech 1999;69(9):635–54.
[29] Sigmund O, Petersson J. Numerical instabilities in topology optimization: a survey on procedures dealing with checkerboard, mesh-dependence and local minima. Struct Multidiscip Optim 1998;16:68–75.
[30] Guest JK, Prevost JH, Belytschko T. Achieving minimum length scale in topology optimization using nodal design variables and projection functions. Int J Numer Meth Eng 2004;61(2):238–54.
[31] Bruns TE. A re-evaluation of the SIMP method with filtering and an alternative formulation for solid-void topology optimization. Struct Multidiscip Optim 2005;30:428–36.
[32] Sigmund O. Morphology-based black and white filters for topology optimization. Struct Multidiscip Optim 2007;33(4):401–24.
[33] Almeida SRM, Paulino GH, Silva ECN. A simple and effective inverse projection scheme for void distribution control in topology optimization. Struct Multidiscip Optim 2009;39(4):359–71.
[34] Choi K, Kim N. Structural Sensitivity Analysis and Optimization 1. Springer; 2005.
[35] Ditlevsen O, Madsen HO. Structural Reliability Methods. Chichester: Wiley; 1996.
[36] Stromberg LL, Beghini A, Baker WF, Paulino GH. Application of layout and topology optimization using pattern gradation for the conceptual design of buildings. Struct Multidiscip Optim 2011;43(2):165–80.